C. R. Physique 15 (2014) 126–139

Contents lists available at ScienceDirect

Comptes Rendus Physique

www.sciencedirect.com

Electron microscopy / Microscopie électronique

Interferometric methods for mapping static electric and magnetic fields

Méthodes interférométriques pour cartographier des champs électriques et magnétiques statiques

Giulio Pozzi [a,*], Marco Beleggia [b], Takeshi Kasama [b], Rafal E. Dunin-Borkowski [c]

[a] *University of Bologna, Department of Physics and Astronomy, viale B. Pichat 6/2, 40127 Bologna, Italy*
[b] *Center for Electron Nanoscopy, Technical University of Denmark, DK-2800 Kgs. Lyngby, Denmark*
[c] *Ernst Ruska-Centre for Microscopy and Spectroscopy with Electrons and Peter Grünberg Institute, Forschungzentrum Jülich, 52425 Jülich, Germany*

ARTICLE INFO

Article history:
Available online 1 February 2014

Keywords:
Transmission electron microscopy
Electron holography
Field mapping
Electric fields
Magnetic fields

Mots-clés :
Microscopie électronique en transmission
Holographie électronique
Cartographie de champs
Champs électriques
Champs magnétiques

ABSTRACT

The mapping of static electric and magnetic fields using electron probes with a resolution and sensitivity that are sufficient to reveal nanoscale features in materials requires the use of phase-sensitive methods such as the shadow technique, coherent Foucault imaging and the Transport of Intensity Equation. Among these approaches, image-plane off-axis electron holography in the transmission electron microscope has acquired a prominent role thanks to its quantitative capabilities and broad range of applicability. After a brief overview of the main ideas and methods behind field mapping, we focus on theoretical models that form the basis of the quantitative interpretation of electron holographic data. We review the application of electron holography to a variety of samples (including electric fields associated with *p–n* junctions in semiconductors, quantized magnetic flux in superconductors and magnetization topographies in nanoparticles and other magnetic materials) and electron-optical geometries (including multiple biprism, amplitude and mixed-type set-ups). We conclude by highlighting the emerging perspectives of (i) three-dimensional field mapping using electron holographic tomography and (ii) the model-independent determination of the locations and magnitudes of field sources (electric charges and magnetic dipoles) directly from electron holographic data.

RÉSUMÉ

La cartographie de champs électriques et magnétiques statiques avec une sonde d'électrons à un niveau de résolution et de sensibilité suffisant pour révéler des variations à l'échelle nanométrique requiert l'utilisation de méthodes sensibles à la phase, telles que la technique de l'ombrage, l'imagerie cohérente en mode de Foucault ou l'équation de transport de l'intensité (TIE). Parmi ces différentes approches, l'holographie électronique «hors axe» en microscopie électronique à transmission joue un rôle prépondérant, en raison de son caractère quantitatif et de son vaste domaine d'utilisation. Après une brève revue des principales idées et méthodes sous-jacentes, nous nous attacherons à décrire les modèles théoriques qui constituent le fondement de l'interprétation quantitative des données holographiques. Nous passerons rapidement en revue l'utilisation de l'holographie électronique pour étudier un grand nombre d'échantillons avec leurs champs électriques et

* Corresponding author.

1631-0705/$ – see front matter
http://dx.doi.org/10.1016/j.crhy.2014.01.005

magnétiques associés : jonctions p–n dans les semi-conducteurs, lignes de flux magnétique quantifié dans les supraconducteurs, topographies du champ magnétique dans et autour de nanoparticules et autres... Les aspects relatifs aux géométries utilisées en optique électronique (doubles biprismes et dispositifs mixtes pour jouer sur la phase et l'amplitude) sont aussi mentionnés. Enfin, nous identifions plusieurs perspectives émergentes de grand intérêt : (i) la cartographie tridimensionnelle de champs en associant tomographie et holographie, (ii) la détermination de la position et de l'intensité de sources de champ (charges électriques et dipôles magnétiques) directement à partir des données holographiques.

1. Introduction

Recent improvements in the basic elements of the transmission electron microscope (TEM) are leading to a renaissance of the instrument, which is regaining a prominent role in the investigation of the nanoworld. These improvements include: (i) the development of Schottky and cold field emission electron guns with unprecedented brightness and coherence, (ii) hardware correction of lens aberrations and (iii) the availability of large semiconductor-based detectors that have single-electron sensitivity.

Significant changes have also resulted from the transition from rigid general-purpose microscopes (optimized for high-resolution work and structure analysis) to custom-made instruments that are designed to fit the needs of a particular research area. As a result, the most advanced research microscopes now play the role of versatile electron-optical benches, offering the option of inserting additional specimen stages and elements (such as electron biprisms, correctors and filters) at several locations in the column. This flexibility provides new exciting opportunities for the inventive researcher, especially for the investigation and mapping of electric and magnetic fields within and around the specimen at the superatomic or mesoscopic length scale. Such research has previously been hampered by the lack of flexibility of conventional TEMs.

In the first part of this paper, we discuss the phase-object approximation (POA), its limits of validity and theoretical models that have been developed for the interpretation of experimental data. Then, after a short review of the field mapping techniques and methodologies that have been proposed and developed over many decades, such as the Schlieren shadow technique and more recent approaches based on coherent Foucault (cF) imaging and the Transport of Intensity Equation (TIE), we focus on what we consider to be the superior technique: the TEM mode of image-plane or in-focus off-axis electron holography [1]. This method provides a unique capability for recovering both the amplitude and the phase of the object wavefunction. In this way, most of the information that is encoded in the electron beam by the specimen can be recovered, allowing projected electric and magnetic fields to be mapped quantitatively. Finally, we discuss the prospect of three-dimensional field mapping using electron holographic tomography and recently developed model-independent methods for determining the locations and magnitudes of field sources (electric charges and magnetic dipoles). In the present paper, we do not discuss non-interferometric techniques based on Lorentz TEM, which are described elsewhere, both in books, *e.g.* [2] and in review articles, *e.g.* [3].

2. The phase-object approximation and its limits of validity

The standard formulation of the phase-object approximation, whose derivation is presented in, *e.g.*, Ref. [4], leads to the representation of the electromagnetic field between planes z_i and z_{i+1} along the optic axis z as a thin phase object, which is characterized by a transmission function T that can be written in the form:

$$T(X,Y,z_i) = \mathrm{e}^{\mathrm{i}\phi(X,Y,z_i)} = \exp\left[\frac{\mathrm{i}\pi}{\lambda E}\int_{z_i}^{z_{i+1}} V(X,Y,z)\,\mathrm{d}z - \frac{2\mathrm{i}\pi e}{h}\int_{z_i}^{z_{i+1}} A_z(X,Y,z)\,\mathrm{d}z\right] \tag{1}$$

where the integrals are taken along a trajectory parallel to the optic axis (directed along the motion of the electrons), $V(X,Y,z)$ is the electrostatic potential, $A_z(X,Y,z)$ is the z-component of the magnetic vector potential $\mathbf{A}$ (which is linked to the magnetic induction $\mathbf{B}$ by the relation $\mathbf{B} = \nabla \times A$) and e, λ, h and E are the absolute values of the electron charge, the de Broglie electron wavelength, the Planck constant and the accelerating voltage of the electron microscope in the non-relativistic approximation, respectively. In order to include the whole field, the integration in Eq. (1) is performed between $-\infty$ and $+\infty$ and the z_i coordinate can be taken to be coincident with the specimen or object plane. Relativistic correction can be included by using appropriate values for λ and E. As the effect of tilting the plane wave is generally negligible at high incident electron energies, the transmission function in Eq. (1) holds for generic illumination. Moreover, the "absorption" of electrons in a very thick specimen or from large-angle scattering and subsequent cut-off by an aperture can be accounted for by introducing a real multiplicative amplitude term $a(X,Y)$ in the transmission function of the object in the form:

$$T(X,Y) = a(X,Y)\mathrm{e}^{\mathrm{i}\phi(X,Y)} \tag{2}$$

The justification for the use of the POA to describe the interaction between the electron beam and electromagnetic fields is based on knowledge gained from several case studies, some of which are now described briefly. By applying the POA to the electrostatic potential of an electron biprism, which can be described either as a cylindrical capacitor [5,6] or using the Septier model (as a thin electrically biased wire between two vertical planes) [7], T can be calculated in analytical form [8,9], revealing that the biprism splits the electron wavefunction and allows the coherent superposition of two half-waves, each of which describes the diffraction and refraction of the electrons, originating from a virtual point source, by an opaque half-plane [10]. Very good agreement between theoretical predictions and experimental measurements has been confirmed, both by older [10] and by more recent [11] experiments, suggesting that the POA is applicable in a situation where the (electric) field extends over several microns and its magnitude is on the order of a few kV/m.

Several efforts have been made to justify the POA on conceptually more satisfactory grounds. The scattering of electrons by the electrostatic field of the biprism has been investigated within the framework of scalar diffraction theory developed by Komrska [6] for the case of a weak electrostatic field. In this case, the wavefunction in the observation plane can be expressed in terms of a diffraction integral. However, numerical calculations are necessary to derive the intensity distribution in the out-of-focus pattern. The intensity distribution calculated using the POA and the diffraction integral agree to at least four significant figures using the method of stationary phase, prompting Komrska and Vlachová [12] to confirm the equivalence of the two descriptions.

For the case of a p–n junction that is described by the simple Spivak model [13], with the internal field topography represented by an arctan function, calculations based on the Komrska diffraction integral were carried out by Lo Vecchio and Morandi [14], who found striking disagreement with results calculated using the POA [15]. Their results led them to state that the POA is hardly tenable for the interpretation of experimental data. Experience gained in the analysis of electromagnetic lenses by means of the multislice method [16], as well as continuing interest in the observation of p–n junctions by TEM methods, for which the POA is an invaluable tool, stimulated a reconsideration of the issue [17]. The analysis of results obtained by the multislice approach indicated that the maximum difference between the POA and each of the multislice calculations never exceeds 5×10^{-4}, *i.e.*, all of the calculations agree to four significant figures, as found by Komrska and Vlachová [12] for the case of an electron biprism. As the multislice approach provides a significant improvement over the use of the Komrska diffraction integral, since the action is calculated along a piecewise rectilinear path that approaches the classical electron trajectory in the limit of a very large number of slices, it can be concluded that the POA is validated by this approach and that the discrepancy reported by Lo Vecchio and Morandi [14] arises from an error in their numerical evaluation of the diffraction integral.

An important failure of the POA occurs when it is applied to the macroscopic fields of electromagnetic lenses [16]. In order to recover the results of the wave-optical paraxial theory of electromagnetic lenses [18,19], it is necessary to take into account the z-dependence of the electron energy and wavelength, due to the variation of the electrostatic potential along the axis, as well as to include two additional magnetic terms in the POA [4], which are usually overlooked [20]. These terms are negligible in most other situations, such as for simulations of a fluxon that is aligned parallel to the electron optical axis and perpendicular to the specimen plane [21].

3. Fields and phase-shift models

The analytical models that have been developed for the interpretation of experimental results can be divided approximately into two groups, depending on whether the calculation is performed in real space or in reciprocal (Fourier) space. In real space, the phase shift is calculated by the direct application of Eq. (1) once the electromagnetic field is known. In reciprocal space, the field is first decomposed into Fourier components, which are then integrated to yield the phase shift in reciprocal representation; the final phase shift in real space is then re-obtained by performing an inverse Fourier transform analytically or numerically. The primary advantage of the reciprocal space approach is related to linearity in electromagnetism: if the field sources are stationary, then the resulting static field throughout space is a superposition of elementary (Coulomb or dipole) fields, which, mathematically, can be carried out by exploiting the convolution theorem. Another advantage is provided by the immediate extension of the approach to periodic objects. Furthermore, considering that numerical Fast Fourier transforms can be performed with negligible computational effort, determination of the phase shift in real or reciprocal space is essentially equivalent. Finally, when considering the Fourier projection theorem, the phase shift in reciprocal representation is a two-dimensional slice of a three-dimensional field in Fourier space, which is also a computationally straightforward operation. On the other hand, there are situations when the real space approach remains most convenient, in particular when dealing with electrostatic problems involving images (charged objects in the proximity of interfaces) or objects/interfaces, whose shapes make the Laplace equation separable (*e.g.*, toroids and ellipsoids).

3.1. The electron biprism, the line dipole and charged dislocations

We have mentioned two models for the electron biprism, which produce essentially the same transmission function across the biprism wire, with the different boundary conditions only affecting the value of the angular deflection for a given potential difference. The cylindrical capacitor model has also been used to interpret results obtained from electron holographic studies of charged dislocations [22–24] and to simulate phase images of linear charged dislocations with the line charge aligned parallel or perpendicular to the electron beam [25]. The Septier model has been extended to deal with

eccentric and non-cylindrical biprism wires and, by overlapping line charges of opposite sign [9], to interpret experimental results obtained in the investigation of the so-called electrostatic Aharonov–Bohm effect [26,27].

3.2. Charged dielectric and metallic nanoparticles on conducting films

A simple model that describes the external electrostatic potential around a charged, insulating (opaque) spherical particle that is positioned over a planar, grounded, conducting substrate can be obtained by considering a point charge at a distance from the plane that is approximately equal to the particle radius and satisfying the boundary condition at the surface of the conducting film by using a symmetrically-placed image charge. The field of the charge and its image then give the field in the particle half-space, whereas the field vanishes in the other half-space. This model was first used to interpret out-of-focus images of charged dielectric particles by means of the diffraction integral [6]. Equivalent results (see, *e.g.*, the biprism and *p–n* junction cases) can be obtained in the POA, with the phase shift in real space given by analytical expressions for both horizontal (plan-view) and vertical (side-view) geometries [28]. Charged dielectric particles have been used to investigate the influence of the perturbed reference wave on electron holographic mapping of long-range electromagnetic fields [4,29] and have become a popular test object in electron holography. More recent work has improved the model to take into account the incomplete opacity of the sphere, to include the effect of the internal field [30,31], to make use of this model for the analysis of possible misinterpretation in the holography process [30] and to perform a comparison between off-axis and in-line electron holography [31,32]. An analytical expression for the field can also be found for a point charge in front of a conducting half-plane [33]. In this case, however, the phase is obtained by numerical integration of the equation in real space [34]. When considering metallic nanoparticles, the need to satisfy the laws of electrostatics [35] leads to a different solution for the field and the corresponding phase shift, which has been found using two complementary approaches, one based on solving the Laplace equation by separating variables in spherical coordinates for constant charge and the other by using an iterative image method for constant potential [36].

3.3. Biased nanowires and metallic tips

A description of a charged nanowire as a line of charges can be used to provide an analytical expression for the field [33] and the phase in real space when the charge density distribution is constant [37] or linear [38]. In order to ensure charge neutrality, an image charge should be introduced, for example with the symmetry plane perpendicular to the line charge playing the role of a grounded electrode. It turns out that equipotential surfaces around a line charge can have ellipsoidal shapes near the tip and can therefore also be used to describe charged ellipsoidal metallic tips [37]. When the aspect ratio is very high, the model can then also be applied to the study of nanowires [38]. By varying the charge density from that of a constant or linear distribution, a cylindrical equipotential surface of fixed radius capped by a hemisphere of the same radius can be approximated, in order to obtain a better model for a nanowire [39]. In addition to their interest for applications, *in situ* experiments on metallic tips [37] have demonstrated strikingly that electron holographic contour maps do not in general represent the potential distribution directly and that the effect of the perturbed reference wave is important and should be taken into account [4].

3.4. Reverse-biased p–n junctions

The potential across and around a reverse-biased *p–n* junction in a thin slab can be described in its simplest form by the Spivak model [13], with the internal field topography connecting to a similar, z-dependent, arctan function in the two half-spaces, satisfying the Laplace equation. Direct integration of Eq. (1) in real space then provides the phase shift in analytical form [15], which can also be obtained using the Fourier space approach [40]. This model was extended by Vanzi [41] to the more general case of a two-sided step junction, also in real space and in analytical form. For a junction lying in a half-plane, as is often encountered in an electron holography experiment where a vacuum region for the reference wave is needed [42,43], the situation is more complicated, as the solution for the field is the electrostatic version of the electromagnetic problem of the diffraction of a plane wave by a thin conducting film [44]. A simpler approach to tackle the same problem, which was found by Gori [45], has provided the key to finding an analytical solution for the electrostatic problem [46]. The Fourier space method allows the components of the phase shift to be calculated in analytical form, reducing the computing time substantially [47]. The same approach has been used to model charged layers in semiconducting specimens, in order to interpret puzzling features observed in electron holography experiments [48]. Unexpectedly, experiments aimed at providing a quantitative examination of reverse-biased *p–n* junctions showed little agreement with theoretical predictions [49]. Part of the discrepancy, which remains unsolved, may originate from the effect of charges on the dielectric layers at the specimen surfaces, as evidenced by numerical results from semiconductor device simulators [50,51] and finite element calculations [52], revealing the key role of the surface potential in establishing the equilibrium charge density within the junction. Another source of systematic error is likely to be associated with the generation of specimen currents by the illuminating electron beam (from secondary electron emission and/or electron–hole pair generation), which may effectively forward-bias the junction and lower the built-in potential [53]. Significant effort is presently being devoted to bridging the gap between electron holography measurements and results from macroscopic transport measurements, in order to understand and demonstrate the quantitative capability of the technique.

3.5. Superconducting vortices

The first model for a superconducting vortex described it as a flux tube in a thin diamagnetic slab, with the two ends of the tube generating a monopolar field in the two vacuum half-spaces above and below it [21]; a clever application of Stokes' theorem [54] was then used to derive the phase shift for a tilted specimen in analytical form. This elementary solution was refined by distributing flux tubes according to the London or Clem field topographies to mimic the structure of the vortex core. Although this improvement did not take into account the bending of the field lines near the specimen surface, it was key to interpreting experimental results obtained using phase contrast methods [55–57]. Even though the real space approach has been used to interpret many features of experiments on conventional type II superconductors [58], including vortex deformation by defect pinning [59] and the finite thickness of the specimen [60], it showed its limits in the investigation of high temperature superconductors, where anisotropy and exotic structures such as pancake vortices [61] play a dominant role [62]. A more satisfying solution was found by using the Fourier space approach [63], first motivated by the need to interpret flux line lattices [64]. The reciprocal framework did not suffer from some of the limitations of the real space approach and proved to be a valuable tool for interpreting complex structures in high T_c and anisotropic materials, such as the pinning of vortices at columnar defects [65,66], pancake vortices [67], Josephson vortices [68] and kinked vortices [69]. By making use of knowledge gained from Fourier space simulations performed for a p–n junction in a half-plane, it was possible to analyze the case of a Pearl vortex near a specimen edge and to explain the reduction of the otherwise quantized flux associated with it [70].

3.6. Simple magnetic models in real space

Calculation of the phase shift of a magnetic dipole in real space using Eq. (1) is elementary, as is its extension to a line of aligned dipoles, *i.e.*, a flux tube or a magnetic needle [29], while the solution for a uniformly magnetized sphere can be found in Ref. [71]. The case of a magnetic bar can be handled easily using Mathematica [72], but the resulting expression is complicated, as shown in Ref. [73], which also describes the case of a tilted slab and a magnetized cylinder. A simple expression for the phase shift of a toroidal magnet (containing a circular magnetization distribution) can be found in a review paper by Olariu and Popescu [74], which is dedicated to experimental and theoretical aspects of the quantum effects of electromagnetic fluxes (the Aharonov–Bohm effect [75]), as demonstrated in a beautiful experiment on shielded magnetic toroids by Tonomura et al. [76]. The expression can also be calculated by considering a toroid of negligible cross-section and integrating the phase shift of the magnetic dipoles aligned along the circular loop. An alternative approach, starting from the magnetic vector potential, involves using elliptic integrals and is much more complicated [35].

3.7. Magnetic nanoparticles and stripe domains in Fourier space

The computation of phase shifts associated with permanently magnetized objects of arbitrary shape can be performed conveniently by introducing a characteristic function $D(\mathbf{r})$ associated with the particle shape, *i.e.*, a function that takes a value of unity inside the particle and zero outside it. Whenever it is possible to perform the Fourier transform of $D(\mathbf{r})$, which is termed $D(\mathbf{k})$ or the shape amplitude, the corresponding phase shift can be derived analytically in reciprocal representation. In this way, in addition to recovering results obtained for simple shapes in real space, it is possible to find the field and phase shift generated by a uniformly magnetized particle of arbitrary shape [77]. This approach has led to an extensive treatment of demagnetization and shape effects in micromagnetism [78], ranging from an analytical solution for the point-function demagnetization tensor for a faceted particle [79,80] to the exact computation of demagnetization factors for important shapes such as disks, elliptic cylinders and rings [81–85], the development of a compact expression for the interaction energy between arbitrarily shaped magnetized objects [86] and, more recently, the calculation of forces and torques between permanent magnets [87,88]. Another benefit of using the Fourier space approach has been the determination of an analytical solution for the phase shift of a series of magnetic stripe domains terminating at the edge of a thin film sample. While this calculation could, in principle, be carried out in real space by considering the distribution of magnetic charges at the sample edge associated with the discontinuity of the magnetization, the Fourier space approach provides a dramatic shortcut towards finding an analytical solution [40]. This model, which is valid for zero domain wall thickness, can easily be extended to more representative magnetization topography profiles across domain walls. In this case, the analytical expression is no longer valid, but the phase shift can still be expressed as a Fourier series with computable coefficients.

4. Shadow, coherent Foucault and TIE methods

The first maps of magnetic fringing fields were obtained by placing a wire [89] or a mesh [90] in the Fresnel region after the specimen: the image of the specimen was then overlapped onto that of the deformed shadow, which could be analyzed to provide quantitative information about the field. This method was improved by inserting an island-structured magnetic field or an amorphous film, which acted as a diffuse scatterer of the transmitted electrons [91]. Recently, in order to measure the electric field distribution around an electrically biased needle, both a holey carbon film with 2-μm-diameter holes arranged in a square lattice of spacing 2 μm (Quantifoil R2/2) and an Au-decorated carbon film were used [92].

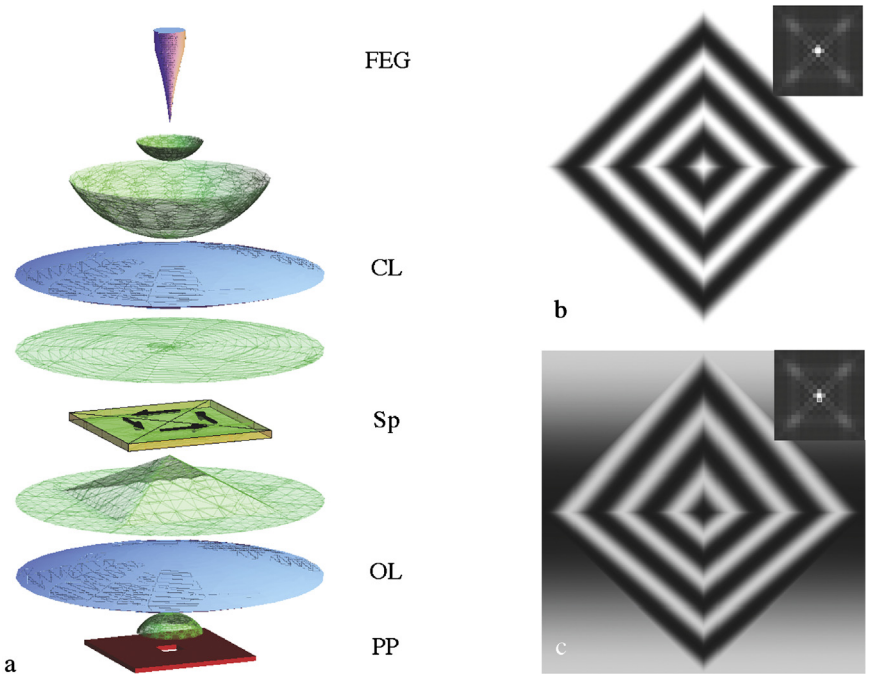

Fig. 1. (Color online.) (a) Schematic diagram illustrating the basis of the coherent Foucault method: FEG, field emission gun; CL, condenser lens system; Sp, specimen; OL, objective lens; PP, phase plate. (b) Coherent Foucault image of a magnetic element with a closure domain structure, generated with a phase plate containing a hole that introduces a phase shift of π centered on the central maximum in the back focal plane (see inset). The diagonal dimension of the magnetic element is chosen to be 2 μm, while the pyramidal phase shift corresponds to that of a 30-nm-thick film of permalloy. (c) Coherent Foucault image generated with the phase plate displaced slightly downwards from the central pixel (marked by a white square in the inset).

The shadow of the electron biprism has also been used in both conventional [93,94] and field emission TEMs to investigate and measure magnetic domain wall widths [95,96].

A field emission TEM is required for the implementation of the coherent Foucault method of imaging, which is described schematically in Fig. 1(a). A spherical wave emitted from the field emission gun (FEG) is transformed by the condenser lens (CL) system into a plane wave impinging on the specimen (Sp), which is chosen here to be a small square magnetic element that contains four domains in a closure structure. The diagonal dimension of the magnetic element is 2 μm and the pyramidal phase shift encoded in the object wavefunction corresponds to that of 30-nm-thick permalloy [97]. In the back focal plane of the objective lens (OL), a phase plate (PP), which is typically fabricated from a thin silicon nitride membrane, is used to introduce a phase shift of π between the low- and high-frequency portions of the spectrum by a small ion-mill drilled hole positioned near the transmitted beam. A simulation of the effect of the phase plate on the image is shown in Fig. 1(b) for a square hole placed symmetrically on top of the central maximum in the back focal plane (see inset) and in Fig. 1(c) the same hole placed just below the transmitted beam. The slight displacement of the hole introduces a change in the contrast of the fringes, as well as some contrast in the area around the square, that could possibly be misinterpreted as indicating the presence of a non-existent fringing field. A careful analysis of the method, discussing its sensitivity to the position and dimensions of the phase plate, is presented in Ref. [97]. It turns out that in the ideal case of a negligibly small hole placed symmetrically, the resulting image displays fringes that, similarly to an electron holographic contour map, are separated by a magnetic flux of h/e, thereby providing quantitative magnetic information directly from the image [97–99]. By assuming that the magnetization is in the plane of an untilted specimen and that there is no fringing field, the spacing of the fringes Δs is given by the expression

$$\Delta s = \frac{h}{eB_0 t} \tag{3}$$

where B_0 is the saturation magnetic induction and t is the magnetic thickness of the specimen. An advantage of the technique over electron holography is that no further processing of the image is required, meaning that *in situ* studies are possible [100,101]. The technique may not be applicable to studies of ultrathin films if the separation of the fringes is larger than the magnetic features of interest.

A non-interferometric phase retrieval method that is gaining in popularity relies on the so-called TIE (for a review see [102]). When applied to magnetic specimens, it allows the magnetization to be recovered and mapped [103–105] and its consistency with electron holography has been assessed [106,107]. However, it has recently been reported, for superconducting vortices, that, contrary to expectations, the method does not provide a model-free method to determine their magnetic structure [108].

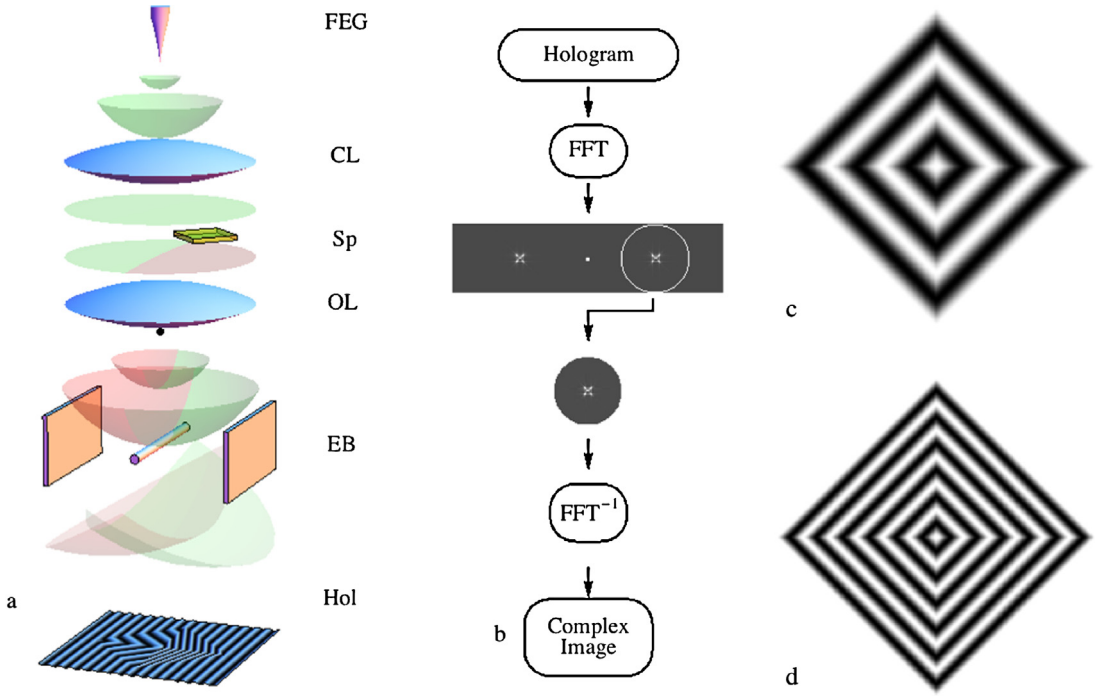

Fig. 2. (Color online.) Schematic diagram illustrating the basis of off-axis electron holography. (a) Hologram recording: FEG, field emission gun; CL, condenser lens system; Sp, specimen; OL, objective lens; EB, electron biprism; Hol, hologram. (b) Hologram processing. (c) Cosine map of the phase, generated for the same magnetic element that was shown in Fig. 1. (d) Cosine map of the two-times amplified phase.

5. Electron holography

In this section, we present an overview of progress in the field of electron interferometry and electron holography after 1980. The early pioneering papers in this field, mainly from the Tübingen group led by Möllenstedt and the Hitachi group led by Tonomura, are reviewed in Ref. [109]. Since then, in large part as a result of the introduction of high brightness and coherent electron sources, in spite of several shortcomings, the most successful electron interferometry device has been the electron biprism [5]. When using a single electron biprism, the interference distance, field of view and fringe spacing are not independent of one another, Fresnel diffraction fringes from the edges of the biprism perturb the image and, more importantly when studying long-range electromagnetic fields, the reference wave is perturbed by the field itself [4]. Applications of electron holography to high-resolution and field mapping have been overwhelming, as testified by several books (*e.g.*, [110–112]), book chapters (*e.g.*, [113–115]) and review articles (*e.g.*, [116–121]).

5.1. The basic scheme

Fig. 2 shows the basic scheme of (a) the recording, (b) the processing and (c) the image rendering steps involved in off-axis electron holography. As in Fig. 1(a), a plane wave emitted from the FEG and collimated by the condenser lens system impinges on the specimen, which is now off-axis. The back-projected virtual image of the electron biprism (EB) divides the wavefront into two parts, one passing trough the specimen (the object wave) and the other passing either through a field-free region of vacuum close to the specimen or through a structureless and field-free region of the specimen (the reference wave). These two parts of the wavefront, magnified by the objective lens, are brought to overlap by the EB. The hologram (Hol), which forms in the recording plane, comprises interference fringes which encode the amplitude and phase of the object wavefunction in their amplitude and phase. In order to recover this information, Fig. 2(b), the hologram is processed using optical or digital means. In the latter case, first a Fast Fourier Transform (FFT) of the hologram is calculated. The FFT contains three key features: a center band and two side bands that contain the desired information. The approach involves selecting one of the sidebands, masking it using a suitable aperture (white circle) and moving it to the origin of Fourier space. An inverse FFT then allows the real and imaginary parts of the complex image and thus the amplitude and phase to be recovered. As a specimen, we have taken the same phase object as shown in Fig. 1. Fig. 2(c) shows the resulting cosine contour map, with a π phase shift added to match the contrast of Fig. 1(b). As a result of the fact that a copy of the original object wavefunction is now available, many further procedures are now possible, *e.g.*, amplification of the map by a factor of 2, as shown in Fig. 2(d), in order to generate a more accurate representation of the variation in phase across the specimen.

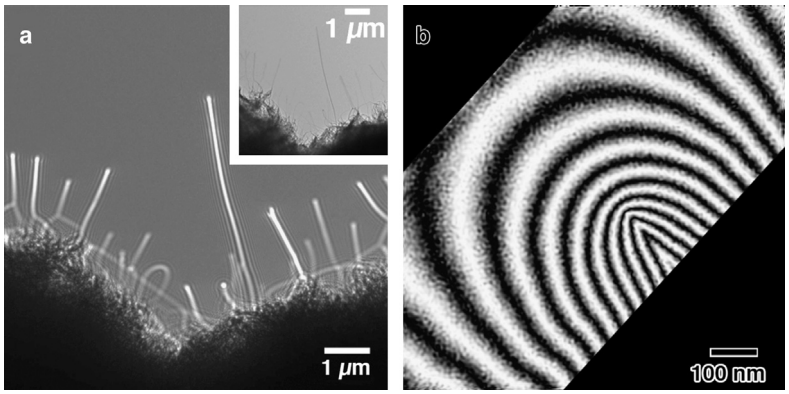

Fig. 3. (a) Fresnel image of an assembly of bundles of single-walled carbon nanotubes biased electrically at 100 V with a gold counter-electrode placed approximately 10 μm from the support. The image was acquired 3 mm overfocus. The inset shows the image in focus. (b) 4× phase amplified cosine contour map of the reconstructed phase around the longest tip, biased electrically at 50 V. The width of the overlap region is approximately 600 nm, and only about a twentieth of the nanotube bundle is captured. The black regions correspond to areas outside the holographic interference fringe pattern, where no phase information could be recovered.

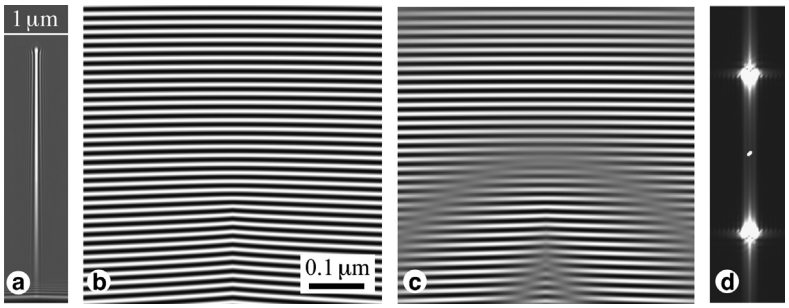

Fig. 4. (a) Simulated Fresnel (3 mm overfocus) image of a 4 μm line of charges with a linearly increasing charge density along its length of 2.5×10^{-4} e/nm^2 (biased electrically at 100 V). (b) Simulated hologram of the same charged wire, biased electrically at 50 V, with 600/32 nm fringe spacing (much larger than in the experiments for clarity of the illustration). (c) Double exposure hologram obtained by summing the hologram in (b) with an empty hologram revealing projected equipotential contours from the resulting moiré pattern. (d) Spectrum of the ideal hologram, calculated as Fourier transform of (b).

5.2. An electron holography case study: the electric field around an electrically biased carbon nanotube

In order to illustrate how a real electron hologram can be recorded and reconstructed to extract a phase image, we reproduce here a selection of earlier results on the investigation of electrically biased carbon nanotube bundles, carried out in a Philips CM300 field emission gun TEM equipped with an electron biprism and a Lorentz lens [38]. A bright-field overview of the specimen, shown in the inset of Fig. 3(a), reveals faint contrast from a series of bundles of carbon nanotubes. Little or no information is present in the image that can be related directly to the presence of charges and electric fields, even though an electrical bias of 50 V was applied to the specimen when the image was recorded. The fields are, however, revealed in the Fresnel image shown in Fig. 3(a), which was taken at a defocus of 3 mm. In this image, strong contrast from the nanotubes increases with distance from the dark grounded electrode visible in the lower part of the image. Although the contrast results from the presence of electric fields, it is not easily interpretable.

An image-plane electron hologram was taken from the region around the tip of the longest nanotube using a biprism voltage of 150 V, corresponding to a field of view of approximately 600 nm and a holographic interference fringe spacing of ∼3 nm. A 4× phase amplified cosine contour map, which is shown in Fig. 3(b), illustrates the projected electric potential around the tip. A linear ramp has been added to the reconstructed phase to provide a better fit to the expected trend of the field.

As explained in more detail elsewhere [117,118], a linear ramp in a reconstructed phase image may be a misleading feature that can arise from incorrect selection of the center of the sideband, from the presence of a constant electric field or from a perturbed reference wave. Therefore, we used simulations to understand the various steps involved and the possible pitfalls. Our model object comprised a one-dimensional charge density distribution, which varied linearly from a value of zero at a grounded electrode to 1 e/nm at its tip over a distance of 4 μm, when biased at 100 V with a gold counter-electrode placed approximately 10 μm from the support. This charge density distribution was used to generate a Fresnel image for a defocus of 3 mm, which is shown in Fig. 4(a) and resembles the experimental image shown in Fig. 3(a).

An image-plane off-axis electron hologram is an interferogram obtained by overlapping an object wave with a tilted reference wave using an electron biprism inserted in the microscope column. Such a hologram is displayed in Fig. 4(b) for a

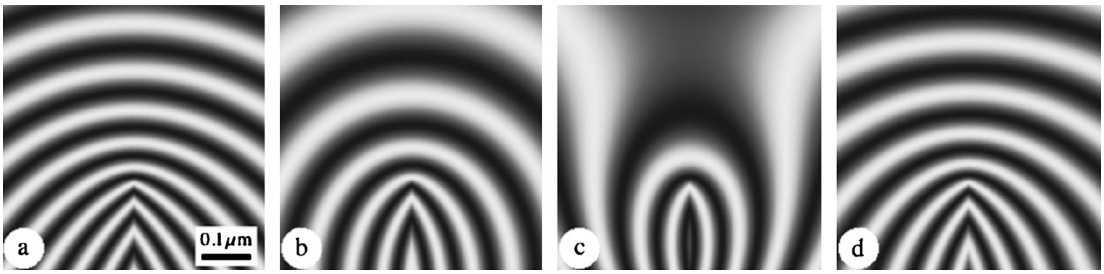

Fig. 5. 4× phase amplified cosine contour maps of (a) the ideal phase image corresponding to the charged wire in Fig. 4(b), (b) the phase image taking into account the perturbation of the reference wave produced by the electric field of the charged object (interference distance 700 nm), (c, d) the perturbed phase image with two different linear ramps.

field of view of 600 nm and a total of 32 interference fringes (compared to 200 in the experimental hologram). The presence of the phase shift due to the projected electrostatic potential can be detected in the form of slight bending of the fringes, especially in the lower part of the image. With 200 fringes, the effect is almost undetectable in the original hologram. Such a hologram is usually obtained together with a so-called vacuum reference hologram, *i.e.*, an interferogram in which the specimen has been taken away and only two-beam holographic interference fringes are present. If the object hologram and reference hologram are superimposed, as in the double-exposure method illustrated in Fig. 4(c), then the resulting moiré fringes allow detection of the phase even without reconstructing the hologram [122].

The reconstruction process normally involves taking the Fourier transform of the hologram, as shown in Fig. 4(d), followed by selecting one of the secondary maxima, which is then filtered and inverse-Fourier-transformed in order to recover the object wavefunction. A sufficiently small interference fringe spacing is required to separate the two lateral spots from the central one without losing any useful information in the filtering step. The process involves using the reference hologram to provide the true origin of Fourier space in the reconstruction and to eliminate coarse distortions introduced by the microscope [117,118,120].

Fig. 5(a) shows a 4× phase amplified cosine contour map of the reconstructed phase. Agreement with the experimental image shown in Fig. 4(b) is not at first sight very satisfying. One reason for the disagreement could be that perturbation of the reference wave caused by the fringing field of the specimen extending to the other side of the biprism has not been taken into account. However, this procedure is not sufficient to remove the difference, as shown in Fig. 5(b), which was calculated for an interference distance [109] of 700 nm. The effect of adding two linear phase ramps is shown in Figs. 5(c, d), illustrating the arbitrariness of the procedure and the variety of phase maps obtainable. In the past, this arbitrariness was corrected by the double-exposure procedure [4,29] and the reason why it does not work in the present case can be found in the fact that in taking the data the reference hologram was probably affected by the electric field of the biased set-up.

An approach that can be used to avoid this additional pitfall involves taking holograms under different conditions (in this case at different bias voltages) so that processing them together leaves only the signal linked to the potential difference between them, as demonstrated in early experiments on *p–n* junctions [42]. Other approaches involve the comparison of theoretical and experimental phases once the linear contributions have been removed, or, as shown in Section 7, to use model-independent measurements of the field sources.

5.3. Multiple biprism set-ups

In order to overcome some of the limitations mentioned above, it has been found to be beneficial to equip a TEM with more than one biprism, in order to allow multiple beam interferometry [123] and holography [124–126] experiments. A clever application of two vertically aligned biprisms was developed by Harada and coworkers, who installed and aligned an upper biprism in the image plane of the objective lens and a second biprism between the crossover point and the image plane of the magnifying lens, thereby providing independent control of the fringe spacing and the width of the interference region [127,128]. An additional advantage of this set-up is that the upper biprism is in focus, while the second biprism is in its geometrical shadow, reducing Fresnel diffraction effects strongly. The same situation can be achieved more cheaply by inserting a fine filament near the specimen [129]. By varying the azimuthal angle between the biprisms, it is also possible to vary both the azimuthal angle of the interference fringes and the vertical length of the interference region, which can be useful for obtaining the phase profile of a one-dimensionally-structured material [130]. When the azimuthal angle between the biprisms is large, it is possible to obtain four-electron-wave interference, which has been used to map electrostatic microfields [131]. Triple-biprism electron interferometry has also been developed, in order to control all of the interference parameters independently [132]. Other arrangements include the twin-electron biprism, which involves the use of two electron biprism wires that are aligned vertically in order to obtain a larger deflection angle without increasing the applied voltage [133] and the trapezoidal biprism, where the wires are parallel to each other and in the same plane, allowing the observation of magnetic fine structure using electron differential holography [134–136]. Another exciting development, which can be used to reduce the problem of the perturbed reference wave experimentally, is referred to as split-illumination electron holography and involves the use of an additional electron biprism in the condenser lens system, in order to increase

the interference distance from a few microns to several tens of microns [137]. Other proposals (*e.g.*, [138,139]) have not yet been realized experimentally.

5.4. Amplitude and mixed-type set-ups

The electron biprism can be classified as a wavefront division electron interferometer. In contrast, single crystal films can, through Bragg diffraction, act as amplitude division beam splitters. When compared with an electron biprism, their main advantages are reduced demand on the coherence of the illuminating electron beam and the absence of Fresnel diffraction phenomena associated with the edges of the biprism. However, they have little versatility, as the angle of the fringes is fixed and transmission of electrons through the single crystal film may lead to unwanted effects. An off-axis out-of-focus or Fresnel holography set-up for mapping the field of a magnetic specimen inserted in the selected area aperture, with a crystal beam splitter located in the normal specimen plane, has demonstrated the feasibility of the method [140], although its resolution was limited by the defocus of the specimen. A similar set-up has been realized with a single crystal beam splitter and the specimen located on different sides of the same grid in the normal specimen plane [141,142]. By using the transmitted beam and two diffracted beams, three electron wave interference has been achieved and used to map the electrostatic field around charged latex particles [143]. The combination of a crystal beam splitter and an electron biprism has also been tested in several set-ups [144–150], but neither this combination nor a double crystal electron interferometer [151] have yet found applications in the mapping of electromagnetic fields.

6. Electron holographic tomography

An exciting prospect is provided by the combination of electron holography with electron tomography, in order to recover three-dimensional fields from their projections, because both contributions to the phase shift in Eq. (1) satisfy the projection requirement for electron tomographic reconstruction [121,152]. After the pioneering papers of Tonomura and coworkers on 3-D reconstruction of electric [153] and magnetic [154] fields, there was little progress for about 20 years, probably due to the demanding requirements of the experiments (requiring the recording of many holograms at different specimen tilt angles) and data processing. In spite of these difficulties, electron holographic tomography, has now been applied successfully to the mapping of electrical potentials in semiconductor junctions [155–158] and the electrostatic potentials of Pt nanoparticles [159]. The acquisition and processing of large numbers of electron holograms has been made easier by the semi-automated acquisition of holographic tilt series [160] and recently applied to the mapping of electrostatic potentials in III–V semiconductor nanowires [161]. The application of electron tomography to magnetic fields, *i.e.*, vector field tomography, is still in its infancy [162–164], with only one experimental study performed using the TIE technique [165]. It should be mentioned that the perturbation of the reference wave in electron holography could be very detrimental in this respect [29].

7. Model-independent measurement of field sources

It has recently been discovered that, by integrating a measured phase image over a circular path that contains a magnetic nanoparticle, a quantity that is directly proportional to the magnetic moment of the particle can be obtained. The measurement of magnetic moments from both simulated and experimental images has been demonstrated and problems related to the presence of neighboring magnetic particles and the perturbation of the holographic reference wave have been discussed [166]. By applying a similar approach to the electrostatic case, it has been possible to measure the charge distribution along a biased carbon nanotube bundle, by starting from the Laplacian of a measured phase image [38]. Work is in progress to assess the performance and limits of these approaches. A first step has been made in this direction, involving the application of aberration-corrected electron holography to measure the charge on an individual nanoparticle to a precision of one elementary unit of charge [167].

8. Conclusions

In this paper, we have reviewed interferometric methods for mapping static electric and magnetic fields in materials in the TEM and highlighted the advantages of off-axis electron holography over other approaches. Such interferometric techniques are increasingly being applied to the characterization of magnetic fields in arrangements of closely-spaced nanocrystals, patterned elements and nanowires, as well as electric fields in field emitters and doped semiconductors.

Future developments in electron holography are likely to involve the introduction of new approaches for enhancing weak magnetic and electric signals based on the automation of lengthy experiments to improve signal to noise in experimental measurements, as well as the combination of electron holography and electron tomography to record both electric and magnetic fields inside nanostructured materials in three dimensions. The characterization of magnetic vector fields inside materials in three dimensions may ultimately require the measurement and subtraction of the unwanted mean inner potential contribution to the measured phase shift at every specimen tilt angle. Other future applications of electron holography may involve the study of dynamic switching processes in spintronic and working semiconductor devices in real time in the presence of multiple stimuli inside the electron microscope.

The unique capability of electron holography to provide quantitative information about static magnetic and electric fields in materials at a resolution approaching (or exceeding) the nanometer scale, coupled with the increasing availability of field emission gun TEMs and quantitative digital recording, ensure that the technique has a very promising future.

Acknowledgements

G.P. gratefully thanks Forschungszentrum Jülich for supporting his research stay. R.D.B. acknowledges financial support from a European Research Council Advanced Grant. The authors acknowledge financial support from the European Union Seventh Framework Programme under Grant Agreement 312483 – ESTEEM2 (Integrated Infrastructure Initiative – I3).

References

[1] J.M. Cowley, Twenty forms of electron holography, Ultramicroscopy 41 (1992) 335–348.
[2] P.B. Hirsch, A. Howie, R. Nicholson, D. Pashley, M.J. Whelan, Electron Microscopy of Thin Crystals, Krieger, Florida, 1977.
[3] J.N. Chapman, The investigation of magnetic domain structures in thin foils by electron microscopy, J. Phys. D, Appl. Phys. 17 (1984) 623–647.
[4] G. Matteucci, G.F. Missiroli, G. Pozzi, Electron holography of long-range electrostatic fields, in: P.W. Hawkes (Ed.), Advances in Imaging and Electron Physics, vol. 122, Elsevier, 2002, pp. 173–249.
[5] G. Möllenstedt, H. Düker, Beobachtungen und Messungen an Biprisma-Interferenzen mit Elektronenwellen, Z. Phys. 145 (1956) 377–397.
[6] J. Komrska, Scalar diffraction theory in electron optics, in: L. Marton (Ed.), Advances in Electronics and Electron Physics, vol. 30, Academic Press, 1971, pp. 139–234.
[7] A. Septier, Bipartition d'un faisceau de particules par un biprisme électrostatique, C. R. Hebd. Séances Acad. Sci., Sér. A B, Sci. Math. Sci. Phys. 249 (1959) 662–664.
[8] G. Matteucci, G. Pozzi, M. Vanzi, Interpretazione d'esperienze d'interferometria elettronica, G. Fis. 20 (1979) 10–21.
[9] G. Matteucci, F.F. Medina, G. Pozzi, Electron-optical analysis of the electrostatic Aharonov–Bohm effect, Ultramicroscopy 41 (1992) 255–268.
[10] J. Komrska, V. Drahoš, A. Delong, Intensity distributions in electron interference phenomena produced by an electrostatic biprism, Opt. Acta: Int. J. Opt. 14 (1967) 147–167.
[11] M.A. Schofield, M. Beleggia, Y. Zhu, G. Pozzi, Characterization of JEOL 2100F Lorentz-TEM for low-magnification electron holography and magnetic imaging, Ultramicroscopy 108 (2008) 625–634.
[12] J. Komrska, B. Vlachová, Justification of the model for electron interference produced by an electrostatic biprism, Opt. Acta: Int. J. Opt. 20 (1973) 207–215.
[13] G.V. Spivak, G.V. Saparin, N.N. Sedov, L.F. Komolova, On the theory of the contrast in a scanning-electron-microscope image of a *p–n* junction, Bull. Acad. Sci. U.S.S.R., Phys. Ser. 32 (1968) 1046–1051.
[14] G. Lo Vecchio, G. Morandi, On the interpretation of TEM images of *p–n* junctions, Phys. Status Solidi A 51 (1979) 383–390.
[15] C. Capiluppi, P. Merli, G. Pozzi, Theoretical model for interpreting TEM images of thinned *p–n* junctions, Optik 47 (1977) 205–214.
[16] G. Pozzi, Multislice approach to lens analysis, in: P.W. Hawkes (Ed.), Advances in Imaging and Electron Physics, vol. 93, Elsevier, 1995, pp. 173–218.
[17] G. Pozzi, On the interpretation of TEM images of *p–n* junctions: a multislice approach, Phys. Status Solidi A 156 (1996) K1–K4.
[18] W. Glaser, Grundlagen der Elektronenoptik, Springer, Wien, 1952.
[19] W. Glaser, P. Schiske, Elektronenoptische Abbildung auf Grund der Wellenmechanik. I, Ann. Phys. 447 (1953) 240–266.
[20] D. Wohlleben, Magnetic phase contrast, in: U. Valdrè (Ed.), Electron Microscopy in Material Science, Academic Press, New York, 1971, pp. 712–757.
[21] A. Migliori, G. Pozzi, Computer simulations of electron holographic contour maps of superconducting flux lines, Ultramicroscopy 41 (1992) 169–179.
[22] D. Cherns, C.G. Jiao, Electron holography studies of the charge on dislocations in GaN, Phys. Rev. Lett. 87 (2001) 205504.
[23] D. Cherns, C.G. Jiao, H. Mokhtari, J. Cai, F.A. Ponce, Electron holography studies of the charge on dislocations in GaN, Phys. Status Solidi B 234 (2002) 924–930.
[24] C. Jiao, D. Cherns, Investigation of the charge on threading edge dislocations in GaN by electron holography, J. Electron Microsc. 51 (2002) 105–112.
[25] D. Cavalcoli, G. Matteucci, M. Muccini, Simulation of electron holographic contour maps of linear charged dislocations, Ultramicroscopy 57 (1995) 385–390.
[26] G. Matteucci, G.F. Missiroli, G. Pozzi, A new electrostatic phase-shifting effect, Ultramicroscopy 10 (1982) 247–251.
[27] G. Matteucci, G. Pozzi, New diffraction experiment on the electrostatic Aharonov–Bohm effect, Phys. Rev. Lett. 54 (1985) 2469–2472.
[28] G. Matteucci, G. Missiroli, G. Pozzi, Simulations of electron holograms of long range electrostatic field, Scanning Microsc. 11 (1997) 367–374.
[29] G. Matteucci, G. Missiroli, E. Nichelatti, A. Migliori, M. Vanzi, G. Pozzi, Electron holography of long-range electric and magnetic fields, J. Appl. Phys. 69 (1991) 1835–1842.
[30] B. Frost, T. Jenkins, On the interpretation of magnetic and electric fields imaged by low-magnification off-axis electron holography, J. Microsc. 187 (1997) 85–95.
[31] T. Latychevskaia, P. Formanek, C.T. Koch, A. Lubk, Off-axis and inline electron holography: Experimental comparison, Ultramicroscopy 110 (2010) 472–482.
[32] C.T. Koch, A. Lubk, Off-axis and inline electron holography: A quantitative comparison, Ultramicroscopy 110 (2010) 460–471.
[33] E. Durand, Électrostatique, vol. 2, Masson, Paris, 1964.
[34] J.W. Chen, G. Matteucci, A. Migliori, G.F. Missiroli, E. Nichelatti, G. Pozzi, M. Vanzi, Mapping of microelectrostatic fields by means of electron holography: theoretical and experimental results, Phys. Rev. A 40 (1989) 3136–3146.
[35] J.D. Jackson, Classical Electrodynamics, 3rd edition, Wiley, New York, 1999.
[36] M. Beleggia, G. Pozzi, Phase shift of charged metallic nanoparticles, Ultramicroscopy 110 (2010) 418–424.
[37] G. Matteucci, G.F. Missiroli, M. Muccini, G. Pozzi, Electron holography in the study of the electrostatic fields: the case of charged microtips, Ultramicroscopy 45 (1992) 77–83.
[38] M. Beleggia, T. Kasama, R.E. Dunin-Borkowski, S. Hofmann, G. Pozzi, Direct measurement of the charge distribution along a biased carbon nanotube bundle using electron holography, Appl. Phys. Lett. 98 (2011) 243101–243103.
[39] J. Cumings, A. Zettl, M.R. McCartney, J.C.H. Spence, Electron holography of field-emitting carbon nanotubes, Phys. Rev. Lett. 88 (2002) 056804.
[40] M. Beleggia, P.F. Fazzini, G. Pozzi, A Fourier approach to fields and electron optical phase-shifts calculations, Ultramicroscopy 96 (2003) 93–103.
[41] M. Vanzi, Theoretical model for studying electrostatic potentials by means of Lorentz microscopy, Optik 68 (1984) 319–333.
[42] S. Frabboni, G. Matteucci, G. Pozzi, M. Vanzi, Electron holographic observations of the electrostatic field associated with thin reverse-biased *p–n* junctions, Phys. Rev. Lett. 55 (1985) 2196–2199.
[43] S. Frabboni, G. Matteucci, G. Pozzi, Observation of electrostatic fields by electron holography: the case of reverse-biased *p–n* junctions, Ultramicroscopy 23 (1987) 29–37.

[44] M. Born, E. Wolf, Principles of Optics: Electromagnetic Theory of Propagation, Interference and Diffraction of Light, 4th edition, Pergamon Press, Oxford, 1969.
[45] F. Gori, Diffraction from a half-plane. A new derivation of the Sommerfeld solution, Opt. Commun. 48 (1983) 67–70.
[46] M. Beleggia, R. Capelli, G. Pozzi, A model for the interpretation of holographic and Lorentz images of tilted reverse-biased *p–n* junctions in a finite specimen, Philos. Mag., B 80 (2000) 1071–1082.
[47] P.F. Fazzini, G. Pozzi, M. Beleggia, Electron optical phase-shifts by Fourier methods: analytical versus numerical calculations, Ultramicroscopy 104 (2005) 193–205.
[48] F. Ubaldi, G. Pozzi, T. Kasama, M. McCartney, S. Newcomb, R.E. Dunin-Borkowski, Interpretation of electron beam induced charging of oxide layers in a transistor studied using electron holography, J. Phys. Conf. Ser. 209 (2010) 012064.
[49] M. Beleggia, D. Cristofori, P.G. Merli, G. Pozzi, Electron microscopy of reverse biased *p–n* junctions, Micron 31 (2000) 231–236.
[50] M. Beleggia, P.F. Fazzini, P.G. Merli, G. Pozzi, Influence of charged oxide layers on TEM imaging of reverse-biased *p–n* junctions, Phys. Rev. B 67 (2003) 045328.
[51] P.F. Fazzini, P.G. Merli, G. Pozzi, F. Ubaldi, Effects of beam–specimen interaction on the observation of reverse-biased *p–n* junctions by electron interferometry, Phys. Rev. B 72 (2005) 085312.
[52] P.K. Somodi, A.C. Twitchett-Harrison, P.A. Midgley, B.E. Kardinal, C.H.W. Barnes, R.E. Dunin-Borkowski, Finite element simulations of electrostatic dopant potentials in thin semiconductor specimens for electron holography, Ultramicroscopy 134 (2013) 160–166.
[53] L. Houben, M. Luysberg, T. Brammer, Illumination effects in holographic imaging of the electrostatic potential of defects and *pn* junctions in transmission electron microscopy, Phys. Rev. B 70 (2004) 165313.
[54] A. Migliori, G. Pozzi, A. Tonomura, Computer simulations of electron holographic contour maps of superconducting flux lines II. The case of tilted specimens, Ultramicroscopy 49 (1993) 87–94.
[55] K. Harada, T. Matsuda, J. Bonevich, M. Igarashi, S. Kondo, G. Pozzi, U. Kawabe, A. Tonomura, Real-time observation of vortex lattices in a superconductor by electron microscopy, Nature 360 (1992) 51–53.
[56] J.E. Bonevich, K. Harada, T. Matsuda, H. Kasai, T. Yoshida, G. Pozzi, A. Tonomura, Electron holography observation of vortex lattices in a superconductor, Phys. Rev. Lett. 70 (1993).
[57] J.E. Bonevich, K. Harada, H. Kasai, T. Matsuda, T. Yoshida, G. Pozzi, A. Tonomura, Lorentz microscopy of vortex lattices (flux lines) in niobium, Phys. Rev. B 49 (1994) 6800–6807.
[58] J. Bonevich, D. Capacci, K. Harada, H. Kasai, T. Matsuda, R. Patti, G. Pozzi, A. Tonomura, Measurement of London penetration depth from holographic images of superconducting vortices: the influence of specimen thickness, Phys. Rev. B 57 (1998) 1200–1205.
[59] S. Fanesi, G. Pozzi, J.E. Bonevich, O. Kamimura, H. Kasai, K. Harada, T. Matsuda, A. Tonomura, Influence of core misalignment and distortion on the Fresnel and holographic images of superconducting fluxons, Phys. Rev. B 59 (1999) 1426–1431.
[60] R. Patti, G. Pozzi, On the interpretation of Lorentz and holographic interference images of superconducting fluxons: the influence of the specimen thickness, Ultramicroscopy 77 (1999) 163–175.
[61] J.R. Clem, Two-dimensional vortices in a stack of thin superconducting films: a model for high-temperature superconducting multilayers, Phys. Rev. B 43 (1991) 7837–7846.
[62] A. Tonomura, H. Kasai, O. Kamimura, T. Matsuda, K. Harada, Y. Nakayama, J. Shimoyama, K. Kishio, T. Hanaguri, K. Kitazawa, M. Sasase, S. Okayasu, Observation of individual vortices trapped along columnar defects in high-temperature superconductors, Nature 412 (2001) 620–622.
[63] M. Beleggia, G. Pozzi, Observation of superconducting fluxons by transmission electron microscopy: A Fourier space approach to calculate the electron optical phase shifts and images, Phys. Rev. B 63 (2001) 054507.
[64] M. Beleggia, G. Pozzi, On the calculation of the phase shift of superconducting fluxons: from the isolated to the lattice case, Ultramicroscopy 84 (2000) 171–183.
[65] M. Beleggia, G. Pozzi, J. Masuko, N. Osakabe, K. Harada, T. Yoshida, O. Kamimura, H. Kasai, T. Matsuda, A. Tonomura, Interpretation of Lorentz microscopy observations of vortices in high-temperature superconductors with columnar defects, Phys. Rev. B 66 (2002) 174518.
[66] O. Kamimura, H. Kasai, T. Akashi, T. Matsuda, K. Harada, J. Masuko, T. Yoshida, N. Osakabe, A. Tonomura, M. Beleggia, G. Pozzi, J. Shimoyama, K. Kishio, T. Hanaguri, K. Kitazawa, M. Sasase, S. Okayasu, Direct evidence of the anisotropic structure of vortices interacting with columnar defects in high-temperature superconductors through the analysis of Lorentz images, J. Phys. Soc. Jpn. 71 (2002) 1840–1843.
[67] M. Beleggia, G. Pozzi, A. Tonomura, H. Kasai, T. Matsuda, K. Harada, T. Akashi, T. Masui, S. Tajima, Model of superconducting vortices in layered materials for the interpretation of transmission electron microscopy images, Phys. Rev. B 70 (2004) 184518.
[68] M. Beleggia, Electron-optical phase shift of a Josephson vortex, Phys. Rev. B 69 (2004) 014518.
[69] M. Beleggia, G. Pozzi, A. Tonomura, Image simulations of kinked vortices for transmission electron microscopy, Ultramicroscopy 110 (2010) 1428–1433.
[70] G. Pozzi, Electron optical effects of a Pearl vortex near the film edge, Phys. Rev. B 76 (2007) 054510.
[71] T. Hirayama, N. Osakabe, Q. Ru, T. Tanji, A. Tonomura, Electron holographic interference micrograph of a single magnetic-domain particle, Jpn. J. Appl. Phys., Part 1: Regul. Pap. & Short Notes & Rev. Pap. 34 (1995) 3294–3297.
[72] G. Pozzi, Electron holography of long-range electromagnetic fields: a tutorial, in: P.W. Hawkes (Ed.), Advances in Imaging and Electron Physics, vol. 123, Elsevier, 2002, pp. 207–223.
[73] K. Keimpema, H. De Raedt, J. De Hosson, Electron holography image simulation of nanoparticles, J. Comput. Theor. Nanosci. 3 (2006) 362–374.
[74] S. Olariu, I.I. Popescu, The quantum effects of electromagnetic fluxes, Rev. Mod. Phys. 57 (1985) 339–436.
[75] Y. Aharonov, D. Bohm, Significance of electromagnetic potentials in the quantum theory, Phys. Rev. 115 (1959) 485–491.
[76] A. Tonomura, N. Osakabe, T. Matsuda, T. Kawasaki, J. Endo, S. Yano, H. Yamada, Evidence for Aharonov–Bohm effect with magnetic field completely shielded from electron wave, Phys. Rev. Lett. 56 (1986) 792–795.
[77] M. Beleggia, Y. Zhu, Electron-optical phase shift of magnetic nanoparticles: I. Basic concepts, Philos. Mag. 83 (2003) 1045–1057.
[78] M. Beleggia, M. De Graef, On the computation of the demagnetization tensor field for an arbitrary particle shape using a Fourier space approach, J. Magn. Magn. Mater. 263 (2003) L1–L9.
[79] S. Tandon, M. Beleggia, Y. Zhu, M. De Graef, On the computation of the demagnetization tensor for uniformly magnetized particles of arbitrary shape. Part I: Analytical approach, J. Magn. Magn. Mater. 271 (2004) 9–26.
[80] S. Tandon, M. Beleggia, Y. Zhu, M. De Graef, On the computation of the demagnetization tensor for uniformly magnetized particles of arbitrary shape. Part II: Numerical approach, J. Magn. Magn. Mater. 271 (2004) 27–38.
[81] M. Beleggia, M. De Graef, Y.T. Millev, D.A. Goode, G. Rowlands, Demagnetization factors for elliptic cylinders, J. Phys. D, Appl. Phys. 38 (2005) 3333–3342.
[82] M. Beleggia, J.W. Lau, M.A. Schofield, Y. Zhu, S. Tandon, M. De Graef, Phase diagram for magnetic nano-rings, J. Magn. Magn. Mater. 301 (2006) 131–146.
[83] M. Beleggia, M. De Graef, Y. Millev, Demagnetization factors of the general ellipsoid: An alternative to the Maxwell approach, Philos. Mag. 86 (2006) 2451–2466.
[84] M. Beleggia, D. Vokoun, M. De Graef, Demagnetization factors for cylindrical shells and related shapes, J. Magn. Magn. Mater. 321 (2009) 1306–1315.

[85] M. Beleggia, M. De Graef, Y.T. Millev, Magnetostatics of the uniformly polarized torus, Proc. R. Soc. A, Math. Phys. Eng. Sci. 465 (2009) 3581–3604.
[86] M. Beleggia, M. De Graef, General magnetostatic shape–shape interactions, J. Magn. Magn. Mater. 285 (2005) L1–L10.
[87] M. De Graef, M. Beleggia, General magnetostatic shape–shape interaction forces and torques, J. Magn. Magn. Mater. 321 (2009) L45–L51.
[88] D. Vokoun, M. Beleggia, L. Heller, P. Šittner, Magnetostatic interactions and forces between cylindrical permanent magnets, J. Magn. Magn. Mater. 321 (2009) 3758–3763.
[89] L. Marton, Electron optical observation of magnetic fields, J. Appl. Phys. 19 (1948) 863–864.
[90] L. Marton, S. Lachenbruch, Electron optical mapping of electromagnetic fields, J. Appl. Phys. 20 (1949) 1171–1182.
[91] R. Wade, The measurement of magnetic microfields, IEEE Trans. Magn. 12 (1976) 34–39.
[92] K. Sasaki, H. Mori, N. Tanaka, H. Murata, C. Morita, H. Shimoyama, K. Kuroda, Measurement of electric field distribution using a conventional transmission electron microscope, J. Electron Microsc. 59 (2010) S89–S94.
[93] G. Pozzi, G. Missiroli, Interference electron microscopy of magnetic domains, J. Microsc. 18 (1973) 103–108.
[94] S. Martelli, G. Matteucci, M.V. Antisari, Shadow and interference electron microscopy of magnetic domain walls, Phys. Status Solidi A 49 (1978) K103–K107.
[95] G. Pozzi, M. Beleggia, M. Schofield, Y. Zhu, Quantitative shadow technique for the investigation of magnetic domain wall widths, Appl. Phys. Lett. 88 (2006) 152506.
[96] M. Beleggia, M. Schofield, Y. Zhu, G. Pozzi, Quantitative domain wall width measurement with coherent electrons, J. Magn. Magn. Mater. 310 (2007) 2696–2698.
[97] A.B. Johnston, J.N. Chapman, The development of coherent Foucault imaging to investigate magnetic microstructure, J. Microsc. 179 (1995) 119–128.
[98] J.N. Chapman, A.B. Johnston, L.J. Heyderman, S. McVitie, W.A.P. Nicholson, B. Bormans, Coherent magnetic imaging by TEM, IEEE Trans. Magn. 30 (1994) 4479–4484.
[99] J.N. Chapman, A.B. Johnston, L.J. Heyderman, Coherent Foucault imaging: a method for imaging magnetic domain structures in thin films, J. Appl. Phys. 76 (1994) 5349–5355.
[100] S. McVitie, J.N. Chapman, L. Zhou, L.J. Heyderman, W.A.P. Nicholson, In-situ magnetising experiments using coherent magnetic imaging in TEM, J. Magn. Magn. Mater. 148 (1995) 232–236.
[101] A.B. Johnston, J.N. Chapman, B. Khamsehpour, C.D.W. Wilkinson, In-situ studies of the properties of micrometre-sized magnetic elements by coherent Foucault imaging, J. Phys. D, Appl. Phys. 29 (1996) 1419.
[102] D. Paganin, K.A. Nugent, Noninterferometric phase determination, in: P.W. Hawkes (Ed.), Advances in Imaging and Electron Physics, vol. 118, 2001, pp. 85–127.
[103] S. Bajt, A. Barty, K. Nugent, M. McCartney, M. Wall, D. Paganin, Quantitative phase-sensitive imaging in a transmission electron microscope, Ultramicroscopy 83 (2000) 67–73.
[104] M. De Graef, Y. Zhu, Quantitative noninterferometric Lorentz microscopy, J. Appl. Phys. 89 (2001) 7177–7179.
[105] V.V. Volkov, Y. Zhu, Lorentz phase microscopy of magnetic materials, Ultramicroscopy 98 (2004) 271–281.
[106] M. Beleggia, M.A. Schofield, V.V. Volkov, Y. Zhu, On the transport of intensity technique for phase retrieval, Ultramicroscopy 102 (2004) 37–49.
[107] T.J. Bromwich, A. Kohn, A.K. Petford-Long, T. Kasama, R.E. Dunin-Borkowski, S.B. Newcomb, C.A. Ross, Remanent magnetization states and interactions in square arrays of 100-nm cobalt dots measured using transmission electron microscopy, J. Appl. Phys. 98 (2005).
[108] J.C. Loudon, C.J. Bowell, N.D. Zhigadlo, J. Karpinski, P.A. Midgley, Magnetic structure of individual flux vortices in superconducting MgB_2 derived using transmission electron microscopy, Phys. Rev. B 87 (2013) 144515.
[109] G.F. Missiroli, G. Pozzi, U. Valdrè, Electron interferometry and interference electron microscopy, J. Phys. E, Sci. Instrum. 14 (1981) 649–671.
[110] A. Tonomura, L. Allard, G. Pozzi, D. Joy, Y. Ono, Electron Holography, Elsevier Science B.V., 1995.
[111] A. Tonomura, Electron Holography, Springer-Verlag, 1999.
[112] E. Völkl, L.F. Allard, D.C. Joy, Introduction to Electron Holography, Plenum Publishing Corporation, 1999.
[113] A. Tonomura, Electron holography, in: E. Wolf (Ed.), Progress in Optics, vol. 23, Elsevier, 1986, pp. 183–220.
[114] R.E. Dunin-Borkowski, T. Kasama, R. Harrison, Electron holography of nanostructured materials, Royal Society of Chemistry, London, 2007, pp. 53–80.
[115] T. Kasama, R.E. Dunin-Borkowski, M. Beleggia, Electron holography of magnetic materials, in: F.A. Monroy Ramírez (Ed.), Holography—Different Fields of Application, InTech, 2011, pp. 53–80.
[116] A. Tonomura, Applications of electron holography, Rev. Mod. Phys. 59 (1987) 639.
[117] P. Midgley, An introduction to off-axis electron holography, Micron 32 (2001) 167–184.
[118] M. Lehmann, H. Lichte, Tutorial on off-axis electron holography, Microsc. Microanal. 8 (2002) 447–466.
[119] H. Lichte, P. Formanek, A. Lenk, M. Linck, C. Matzeck, M. Lehmann, P. Simon, Electron holography: Applications to materials questions, Annu. Rev. Mater. Res. 37 (2007) 539–588.
[120] H. Lichte, M. Lehmann, Electron holography—basics and applications, Rep. Prog. Phys. 71 (2008) 016102.
[121] P.A. Midgley, R.E. Dunin-Borkowski, Electron tomography and holography in materials science, Nat. Mater. 8 (2009) 271–280.
[122] G. Matteucci, G. Missiroli, J. Chen, G. Pozzi, Mapping of microelectric and magnetic fields with double-exposure electron holography, Appl. Phys. Lett. 52 (1988) 176–178.
[123] T. Kawasaki, G. Missiroli, G. Pozzi, A. Tonomura, Multiple-beam interference experiments with a holographic electron microscope, Optik 92 (1993) 168–174.
[124] T. Kawasaki, G. Pozzi, A. Tonomura, Three-beam electron holography experiments, in: Proc. 13th Int. Congr. on Electron Microscopy—ICEM 13, Paris, 1994, vol. 1, 1994, pp. 323–324.
[125] T. Hirayama, T. Tanji, A. Tonomura, Direct visualization of electromagnetic microfields by interference of three electron waves, Appl. Phys. Lett. 67 (1995) 1185–1187.
[126] T. Hirayama, G. Lai, T. Tanji, N. Tanaka, A. Tonomura, Interference of three electron waves by two biprisms and its application to direct visualization of electromagnetic fields in small regions, J. Appl. Phys. 82 (1997) 522–527.
[127] K. Harada, A. Tonomura, Y. Togawa, T. Akashi, T. Matsuda, Double-biprism electron interferometry, Appl. Phys. Lett. 84 (2004) 3229–3231.
[128] K. Harada, T. Akashi, Y. Togawa, T. Matsuda, A. Tonomura, Optical system for double-biprism electron holography, J. Electron Microsc. 54 (2005) 19–27.
[129] K. Yamamoto, T. Hirayama, T. Tanji, Off-axis electron holography without Fresnel fringes, Ultramicroscopy 101 (2004) 265–269.
[130] K. Harada, T. Akashi, Y. Togawa, T. Matsuda, A. Tonomura, Variable interference azimuth angle in double-biprism electron interferometry, Jpn. J. Appl. Phys., Part 2: Letters 44 (2005) L636–L639.
[131] K. Miyashita, K. Yamamoto, T. Hirayama, T. Tanji, Direct observation of electrostatic microfields by four-electron-wave interference using two electron biprisms, J. Electron Microsc. 53 (2004) 577–582.
[132] K. Harada, T. Matsuda, A. Tonomura, T. Akashi, Y. Togawa, Triple-biprism electron interferometry, J. Appl. Phys. 99 (2006) 113502.
[133] M. Ikeda, A. Sugawara, K. Harada, Twin-electron biprism, J. Electron Microsc. 60 (2011) 353–358.
[134] T. Tanji, T. Hirayama, Differential microscopy in off-axis transmission electron microscope holography, Scanning Microsc. 11 (1997) 417–425.
[135] T. Tanji, S. Manabe, K. Yamamoto, T. Hirayama, Electron differential microscopy using an electron trapezoidal prism, Ultramicroscopy 75 (1999) 197–202.

[136] T. Tanji, S. Manabe, K. Yamamoto, T. Hirayama, Observation of magnetic fine structures by electron differential microscopy, Mater. Charact. 42 (1999) 183–192.
[137] T. Tanigaki, Y. Inada, S. Aizawa, T. Suzuki, H.S. Park, T. Matsuda, A. Taniyama, D. Shindo, A. Tonomura, Split-illumination electron holography, Appl. Phys. Lett. 101 (2012) 043101.
[138] L. Kou, J. Chen, Eliminating the influence of the perturbed reference wave in electron holography, J. Mod. Opt. 42 (1995) 1171–1178.
[139] D. Van Dyck, Through object electron holography, J. Electron Microsc. 48 (1999) 33–34.
[140] G. Matteucci, G.F. Missiroli, G. Pozzi, A new off-axis Fresnel holographic method in transmission electron microscopy: an application on the mapping of ferromagnetic domains. III, Ultramicroscopy 8 (1982) 403–408.
[141] Q. Ru, N. Osakabe, J. Endo, A. Tonomura, Electron holography available in a non-biprism transmission electron microscope, Ultramicroscopy 53 (1994) 1–7.
[142] Q. Ru, Incoherent electron holography, J. Appl. Phys. 77 (1995) 1421–1426.
[143] T. Hirayama, K. Yamamoto, K. Miyashita, T. Saito, Amplitude-division three-electron-wave interference for observing pure phase objects having low spatial frequency, J. Electron Microsc. 54 (2005) 51–55.
[144] G. Matteucci, G.F. Missiroli, G. Pozzi, A "mixed" type electron interferometer. II, Ultramicroscopy 7 (1982) 277–286.
[145] R.A. Herring, G. Pozzi, T. Tanji, A. Tonomura, Realization of a mixed type of interferometry using convergent-beam electron diffraction and an electron biprism, Ultramicroscopy 50 (1993) 94–100.
[146] R.A. Herring, G. Pozzi, T. Tanji, A. Tonomura, Interferometry using convergent electron diffracted beams plus an electron biprism (CBED + EBI), Ultramicroscopy 60 (1995) 153–169.
[147] B.M. Mertens, M.H.F. Overwijk, P. Kruit, Off-axis holography with a crystal beam splitter, Ultramicroscopy 77 (1999) 1–11.
[148] R.A. Herring, Energy-filtered electron-diffracted beam holography, Ultramicroscopy 104 (2005) 261–270.
[149] R.A. Herring, Planar diffracted-beam interferometry/holography, Ultramicroscopy 108 (2008) 688–697.
[150] F. Houdellier, M.J. Hÿtch, Diffracted phase and amplitude measurements by energy-filtered convergent-beam holography (CHEF), Ultramicroscopy 108 (2008) 285–294.
[151] F. Zhou, The principle of a double crystal electron interferometer, J. Electron Microsc. 50 (2001) 371–376.
[152] M. Weyland, P. Midgley, Electron Tomography, Royal Society of Chemistry (RSC) Publishing, Cambridge, UK, 2007.
[153] G. Lai, T. Hirayama, K. Ishizuka, T. Tanji, A. Tonomura, Three-dimensional reconstruction of electric-potential distribution in electron-holographic interferometry, Appl. Opt. 33 (1994) 829–833.
[154] G. Lai, T. Hirayama, A. Fukuhara, K. Ishizuka, T. Tanji, A. Tonomura, Three-dimensional reconstruction of magnetic vector fields using electron-holographic interferometry, J. Appl. Phys. 75 (1994) 4593–4598.
[155] A. Twitchett, T. Yates, R. Dunin-Borkowski, S. Newcomb, P. Midgley, Three-dimensional electrostatic potential of a Si p–n junction revealed using tomographic electron holography, J. Phys. Conf. Ser. 26 (2006) 29.
[156] A.C. Twitchett-Harrison, T.J. Yates, S.B. Newcomb, R.E. Dunin-Borkowski, P.A. Midgley, High-resolution three-dimensional mapping of semiconductor dopant potentials, Nano Lett. 7 (2007) 2020–2023.
[157] A.C. Twitchett-Harrison, R.E. Dunin-Borkowski, P.A. Midgley, Mapping the electrical properties of semiconductor junctions—the electron holographic approach, Scanning 30 (2008) 299–309.
[158] A.C. Twitchett-Harrison, T.J.V. Yates, R.E. Dunin-Borkowski, P.A. Midgley, Quantitative electron holographic tomography for the 3D characterisation of semiconductor device structures, Ultramicroscopy 108 (2008) 1401–1407.
[159] T. Tanigaki, S. Aizawa, T. Suzuki, A. Tonomura, Three-dimensional reconstructions of electrostatic potential distributions with 1.5-nm resolution using off-axis electron holography, J. Electron Microsc. 61 (2012) 77–84.
[160] D. Wolf, A. Lubk, H. Lichte, H. Friedrich, Towards automated electron holographic tomography for 3D mapping of electrostatic potentials, Ultramicroscopy 110 (2010) 390–399.
[161] D. Wolf, H. Lichte, G. Pozzi, P. Prete, N. Lovergine, Electron holographic tomography for mapping the three-dimensional distribution of electrostatic potential in III–V semiconductor nanowires, Appl. Phys. Lett. 98 (2011) 264103.
[162] V. Stolojan, R. Dunin-Borkowski, M. Weyland, P. Midgley, Three-dimensional magnetic fields of nanoscale elements determined by electron-holographic tomography, in: Conference Series—Institute of Physics, vol. 168, Institute of Physics, Philadelphia, 1999, pp. 243–246.
[163] S.J. Lade, D. Paganin, M.J. Morgan, Electron tomography of electromagnetic fields, potentials and sources, Opt. Commun. 253 (2005) 392–400.
[164] C. Phatak, M. Beleggia, M. De Graef, Vector field electron tomography of magnetic materials: theoretical development, Ultramicroscopy 108 (2008) 503–513.
[165] C. Phatak, A.K. Petford-Long, M. De Graef, Three-dimensional study of the vector potential of magnetic structures, Phys. Rev. Lett. 104 (2010) 253901.
[166] M. Beleggia, T. Kasama, R.E. Dunin-Borkowski, The quantitative measurement of magnetic moments from phase images of nanoparticles and nanostructures—I. Fundamentals, Ultramicroscopy 110 (2010) 425–432.
[167] C. Gatel, A. Lubk, G. Pozzi, E. Snoeck, M.J. Hÿtch, Counting elementary charges on nanoparticles by electron holography, Phys. Rev. Lett. 111 (2013) 025501.